Co-Design of Strain-Actuated Solar Arrays for Precision Pointing and Jitter Reduction

Christian M. Chilan*, Daniel R. Herber†, Yashwanth Kumar Nakka‡,
Soon-Jo Chung§, James T. Allison¶
University of Illinois at Urbana-Champaign, Urbana, IL, 61801, USA
Jack B. Aldrich‖, and Oscar S. Alvarez-Salazar**
Jet Propulsion Laboratory, California Institute of Technology, Pasadena, CA, 91109, USA

Many important spacecraft operations require precision pointing such as space astronomy and high-rate communications. Traditionally, reaction wheels have been used for this purpose but they have been considered unreliable for many missions. This work presents the use strain-actuated solar arrays (SASA) for precision pointing and jitter reduction. Piezoelectric actuators can achieve higher precision and bandwidth than reaction wheels, and they can also provide quiet operation for sensitive instruments. The representation of the array dynamics in the studies presented here is based on Euler-Bernoulli beam theory for high-fidelity simulations. This work also presents a methodology for the combined design of distributed structural geometry for the arrays and distributed control system design. The array geometry design allows for a distributed thickness profile, and the control design determines the distributed moment on the array. Fundamental limits on slew magnitude are found using pseudo-rigid body dynamic model (PRBDM) theory. A parametric study based on a representative spacecraft model demonstrates the validity of the proposed approach and illustrates optimal design trends.

I. Introduction

Advancements in spacecraft technology accelerate discovery in Earth and space sciences; faster reorientation and ultra-quiet jitter-free operation for space observatories and optical links have the potential to transform the rate and quality of data obtained for scientific investigation.[1,2] Scientific needs drive exceptionally stringent spacecraft pointing and control requirements, which in turn demand new strategies for space vehicle design and control.[3,4] Traditionally, Reaction Wheel Assemblies (RWAs)—momentum exchanging flywheels—have been used for attitude control but they have been deemed problematic for many science missions because of RWA disturbances and reliability concerns.[5] One alternative control strategy intended to overcome some of these problems used robotic appendages with rigid links.[6] The strategy proposed here uses existing appendages (solar arrays) with distributed actuation to achieve high-precision attitude control. Strain-Actuated Solar Arrays (SASAs), which employ distributed piezoelectric material actuators, provide high accuracy and bandwidth for spacecraft attitude control, thereby supporting quiet operation for high-precision scientific payloads. Additionally, the dual use of the same spacecraft component, i.e. solar arrays, for power generation and precision attitude control reduces payload delivery costs.

What is unique to SASA is its ability to perform attitude slewing maneuvers while simultaneously suppressing structural vibrations. Although the current bending limit of the arrays bounds the magnitude of

*Postdoctoral Research Associate, Aerospace Engineering, 104 S. Wright Street, Urbana, IL, 61801, AIAA Member
†Graduate Student, Industrial and Enterprise Systems Engineering, 104 S. Mathews Ave, Urbana, IL, 61801, AIAA Student Member
‡Graduate Student, Aerospace Engineering, 104 S. Wright Street, Urbana, IL, 61801
§Associate Professor, Aerospace Engineering, 104 S. Wright Street, Urbana, IL, 61801, AIAA Senior Member
¶Assistant Professor, Industrial and Enterprise Systems Engineering, 104 S. Mathews Ave, Urbana, IL, 61801, AIAA Member
‖Senior Member, Guidance and Control Analysis Group, 4800 Oak Grove Drive, M/S 198-326. AIAA Member.
**Manager, Guidance and Control Analysis Group, 4800 Oak Grove Drive, M/S 198-326. AIAA Member.

the attitude maneuvers to the order of milli-radians, these advancements are important for high precision pointing, and when combined with other actuation technology for large reorientations may provide a feasible replacement for RWAs to improve pointing accuracy and reliability.

Strain-actuated solar arrays for precision pointing will require the arrays to behave more like a flexible structure than a rigid one. Space structures by necessity are extremely lightweight and flexible but vibrations from RWAs, reorientation maneuvers, and other disturbances are complex and degrade performance. These factors have given rise to the extensively-studied topic of Control-Structure Interaction (CSI). Most CSI literature has concentrated on reducing structural vibration through active damping,[4,7] i.e., using control systems to actively damp lower-frequency structural vibration modes without exciting higher-frequency modes.[8–10] This design paradigm has led to design heuristics, such as placing actuators according to locations of high strain for important structural modes.[8,11] If the design objective is different from vibration reduction alone (e.g., more sophisticated motion control), then CSI heuristics produce suboptimal results. As an illustrative example, consider Skylab where part of the control effort goes to reducing vibration and getting flexible bodies to behave as rigid bodies, leaving only the remaining control effort for productive tasks.[9] Instead of using the proxy control objective of eliminating flexible behavior, a more elegant solution would be to improve overall system performance by working with elastic dynamics rather than fighting against it. In the integrated design and control study presented here we seek to utilize flexible body dynamics to our advantage to provide new levels of system performance. Instead of using distributed actuation of solar arrays to damp out vibration as the primary objective, it is used to control spacecraft orientation as a primary objective.

The SASA system presented in this article may be classified as an intelligent structure according to the framework established by Wada et al.[12] Active structures utilize point actuation with feedback control, and require precise knowledge of modes to avoid problems with spillover that limit performance.[11,13] Intelligent structures use distributed actuation to control more modes and yield new functionality.[4,14,15] Piezoelectric material actuators (PEMAs)[16–18] are a proven solution for distributed actuation.[14,19] Applying voltage across PEMAs bonded to or embedded within structures induces strain, causing the structure to deform (bend, twist, elongate, or contract depending on design). PEMA-based intelligent structures easily outperform conventional point-actuated structures,[4,20] in terms of mass, cost, and dynamic performance.[21] Here the use of piezoelectric actuators is extended beyond active damping by providing distributed internal moments to the solar arrays for pointing control and jitter reduction.

The distributed nature of intelligent structures provides tremendous design flexibility. This opens up new opportunities for system performance, but also increases design difficulty.[11,21,22] CSI heuristics help manage this complexity, but also implicitly limit performance and prevent engineers from realizing the full capabilities of intelligent structures.[4] In addition, heuristics developed for active damping are not aligned with the objectives of more sophisticated motion control, as is the case with the strain-actuated solar array (SASA) system presented here. Development of design theory and methods congruent with the design problem are needed.

Intelligent structures are highly-coupled systems, yet structural and control aspects are typically designed in sequence,[8,13,23] motivated by the need to simplify the design problem and fit the structure of existing design organizations.[9] Sequential methods cannot fully exploit synergy between structural and control design.[24,25] More recently, co-design (combined physical- and control-system design) has been introduced as a more general methodology that simultaneously optimizes structures and controls without the need for simplifying assumptions. Co-design aids engineers in treating the intelligent structure design problem in a more comprehensive manner.[24] Furthermore, it has been shown that co-design could yield solutions with significant performance improvements[26,27] and at lower costs than CSI iterated sequential methods.[25,28,29]

In most previous co-design studies the physical aspects of the system design have been managed in a very simplified manner. For example, physical system (plant) design decisions have often been limited to actuator placement.[30,31] Many co-design studies have used simplified plant models[9,20,32] that do not support exploration of changes to distributed geometric structural design, preventing full exploitation of the design synergy between structural tailoring and distributed control system design. A more ideal co-design method supports changes to distributed structural properties (e.g., changing structural shape affects how inertial and stiffness properties vary spatially). Structural tailoring coupled with control design has long been recognized as an important, yet formidable problem.[33] Smith, Grigioriadis, and Skelton identified the need to tailor passive system dynamics to work optimally with active control.[9] In their method plant design variables were limited to direct changes to stiffness, damping, and mass matrices. This method was demonstrated using

lumped parameter problems, but cannot be extended to distributed parameter systems.

To summarize, much is known regarding design of control systems and actuators for intelligent structures, but only if the structural design is held fixed. A few examples of fully-integrated design exist, but only with simplified treatment of structural design. To the authors' knowledge, no examples of previous work address intelligent structure design in a fully integrated way that include detailed treatment of structural design. More precisely, while distributed structural shape optimization has been performed to optimize passive dynamic properties,[34,35] distributed structural geometry has not been optimized for active dynamic properties in concert with control system design. In this article we introduce the first instance of such a design strategy. Here distributed geometry—specifically, distributed array structure thickness—is optimized simultaneously with distributed moment control of the array structure.

An initial study of the SASA concept was performed previously, focusing on attitude control, to demonstrate its feasibility.[36] It was shown that the spacecraft bus orientation can be controlled by the appropriate bending of the arrays. This initial study did not address structural design. Bending dynamics were modeled using a pseudo-rigid body dynamic model (PRBDM)[37] with moments over rigid segments as the control input. This type of lumped parameter model is a basic approximation of a spacecraft with strain-actuated arrays, but provides important insights into the design problem due to its intuitive structure. A more accurate, physically consistent description of the array dynamics can be modeled using flexible beam theory. Underactuated control of a flexible array has been demonstrated by applying an external moment to the bus.[38] This work primarily uses the Euler-Bernoulli beam theory for a more accurate, physically consistent description of the array dynamics, and the partial differential equation (PDE) model is implemented using Galerkin approximating functions.[39–41] In the model piezoelectric actuation are represented by a distributed moment on the beam. The model also accounts for elastic and inertial properties of the actuators.

The use of open-loop controls and distributed optimization parameters, e.g. array thickness and control moment, allows solution without making assumptions on the control or physical architecture. This aids exploration of ultimate system performance limits.[25] Although there may be practical constraints for feedback control system implementation, the resulting co-design solutions can provide important insights into how to design the physical array structure such that it performs optimally as an actively controlled system, capitalizing on synergy between physical and control system design.[42] Direct transcription (DT) is the numerical approach used to solve the co-design problems in the studies presented here. DT transforms the infinite dimensional optimal-control problem into a finite nonlinear programming problem.[43–45] Direct transcription avoids the difficulties associated with the derivation and solution of the Euler-Lagrange conditions of the calculus of variations.[45] For instance, DT can find optimal open-loop control trajectories for problems with nonlinear system dynamics, inequality path constraints, and singular arcs. DT has been traditionally used in trajectory optimization.[44,46,47] Recent examples of co-design with DT include actively controlled automotive suspensions,[24] wave energy converters,[48] and wind turbine design.[49]

II. Modeling of the Strain-Actuated Solar Arrays and Rigid Spacecraft Bus

Here we assume that actuation is effected only through solar array strain actuators that produce strain at the solar array structure surface, resulting in array bending and a distributed moment due to strain actuator surface forces. The strain actuators do not interact with anything external to the spacecraft system, so total system momentum must be conserved (in contrast to actuation via thrusters or torque rods). Therefore, for a generally counter clockwise (CCW) movement of the solar array, the bus (θ) will rotate in the opposing CW direction allowing for attitude changes. This is evident in both the illustration of the beam theory coordinate system in Fig. 1a and its comparable PRBDM lumped parameter model in Fig. 1b.

II.A. Partial Differential Equation (PDE) Model

A spacecraft model based on Euler-Bernoulli beam theory is derived here that captures spacecraft dynamics, including planar rigid body motion of the spacecraft body, structural dynamics of the solar arrays, and distributed strain actuation. In fact, our modeling approach was inspired by the recent work on aircraft dynamics with flexible, articulated wings.[50] The spacecraft body is modeled as a simple cylinder, and the solar array structure is modeled as a composite beam with thickness that can vary along its length.

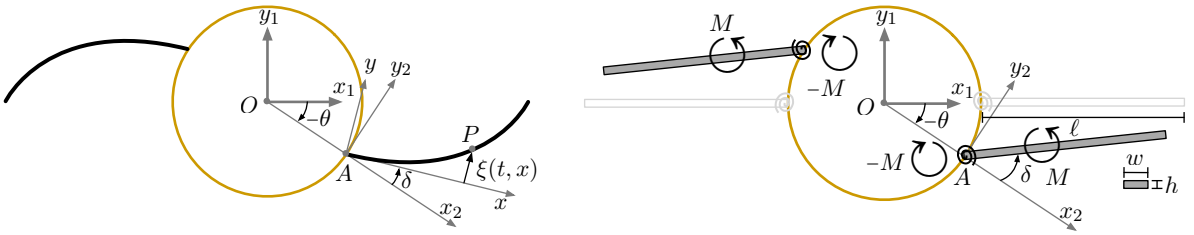

(a) Beam theory model. **(b) Lumped parameter model.**

Figure 1: Illustration of the two modeling approaches used to gain design insights.

II.A.1. PDE Dynamic Model

The coordinate systems used for the derivation of the Lagrangian of the system are shown in Fig. 1a. The model has two arrays with asymmetric actuation. Let the radius of the spacecraft body be r, and the spacecraft body rotation angle about origin O be θ. In deriving the equations of motion, it is assumed that the deflections due to bending are small and the beam has no longitudinal velocity. In the coordinate system attached to the center of the bus, the location of a point P on the beam is given by $R_{P/O} = [x + r, \xi]$ where $\xi(x,t)$ is the displacement due to bending. The beam is laminated with a piezoelectric material on the top surface which has the same width as that of the beam. The Young's modulus of the beam is E. The thickness profile of the beam is denoted $h(x)$. The mass per unit length of the beam $m_R(x)$. The total length and width of the beam are represented by ℓ and w, respectively. The mass moment of inertia of the spacecraft bus is J_θ.

The Lagrangian of the system includes the spacecraft bus as well as the flexible dynamics of the solar arrays:

$$\begin{aligned} L = &\frac{1}{2}J_\theta\dot{\theta}^2 + \int_0^\ell m_R\Big[r^2\dot{\theta}^2 + \dot{\theta}^2\left(x^2+\xi^2\right) + \dot{\xi}^2 + 2r\dot{\xi}\dot{\theta} + 2\dot{\theta}^2 rx + 2\dot{\xi}\dot{\theta}x\Big]dx \\ &- \int_0^\ell EI\left(\xi^{''}\right)^2 dx - \int_0^\ell A_x(\dot{\theta},x)\left(\xi^{'}\right)^2 dx \end{aligned} \tag{1}$$

where $(\cdot)^{'} = \frac{\partial}{\partial x}(\cdot)$ and the second moment of area $I(x)$ is:

$$I(x) = \frac{1}{12}wh^3(x) \tag{2}$$

The axial tension in the beam due to rotation is:

$$A_x\left(\dot{\theta},x\right) = \int_x^\ell \left[m_R\dot{\theta}^2 s\right] ds = p(x)\dot{\theta}^2 \tag{3}$$

The moment applied on the beam is $M(x,t)$. Using the Euler-Lagrangian approach, the equations of motion were derived. The dynamics in the matrix form are:

$$\int_0^\ell [\boldsymbol{M_s}]\begin{bmatrix}\ddot{\theta}\\ \ddot{\xi}\end{bmatrix}dx + \int_0^\ell [\boldsymbol{C_s}]\begin{bmatrix}\dot{\theta}\\ \dot{\xi}\end{bmatrix}dx + \begin{bmatrix}0\\ \int_0^\ell (2EI\xi^{''} + 2\mu EI\dot{\xi}^{''})^{''}dx\end{bmatrix} = \begin{bmatrix}d\\ \int_0^\ell 2M^{''}dx\end{bmatrix} \tag{4}$$

where:
$$[\boldsymbol{M_s}] = \begin{bmatrix}m_{11}(\xi) & m_{12}\\ m_{12} & m_{22}\end{bmatrix} = \begin{bmatrix}\left(J_\theta/\ell + 2\left(m_R\left((x+r)^2+\xi^2\right) - p\xi^{'2}\right)\right) & 2m_R(x+r)\\ 2m_R(x+r) & 2m_R\end{bmatrix}$$

$$[\boldsymbol{C_s}] = \begin{bmatrix}c_{11}(\xi,\dot{\xi}) & c_{12}(\xi,\dot{\theta})\\ -c_{12}(\xi,\dot{\theta}) & 0\end{bmatrix} = \begin{bmatrix}2m_R\xi\dot{\xi} - 2p\xi^{'}\dot{\xi}^{'} & 2m_R\xi\dot{\theta} + 2(p\xi^{'})^{'}\dot{\theta}\\ -2m_R\xi\dot{\theta} - 2(p\xi^{'})^{'}\dot{\theta} & 0\end{bmatrix}$$

The term μ is used to model the damping in the solar array. There is a disturbance d acting on the bus as a torque input. The following boundary conditions of the PDE are due to a fixed root and a free tip of the array:

$$\xi(0,t) = \xi^{'}(0,t) = 0, \qquad EI\left(\xi^{''} + \mu\dot{\xi}^{''}\right)\Big|_{x=\ell} = M(x,t)|_{x=\ell}, \qquad EI\left(\xi^{'''} + \mu\dot{\xi}^{'''}\right)\Big|_{x=\ell} = M^{'}(x,t)\Big|_{x=\ell} \tag{5}$$

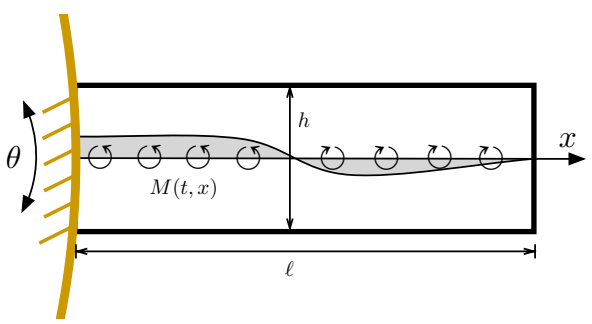

(a) Continuously distributed internal moment on a uniform thickness array.

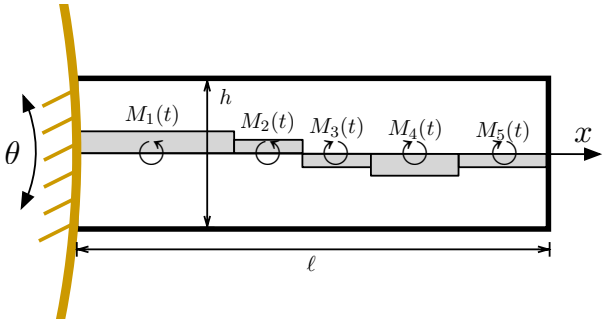

(b) Piecewise constant distributed internal moment on a uniform thickness array.

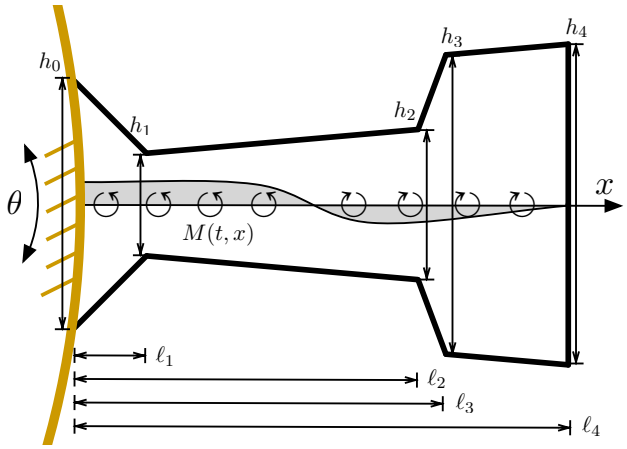

(c) Piecewise linear distributed array thickness.

Figure 2: Various illustrations of internally actuated array design problems for pointing.

II.A.2. Galerkin Formulation

To numerically approximate the PDE in the equations of motion above, we use a Galerkin formulation (see Refs.[40,41,50] for more details on this formulation). The linear combination of the appropriate comparison functions is used to approximate the dynamics of the array and the distributed moment. These functions are chosen such that they satisfy the boundary conditions of the beam, i.e., the fixed-free condition. The jth approximating functions are given by:[40]

$$\phi_j(x) = 1 - \cos\left(\frac{j\pi x}{\ell}\right) + \frac{1}{2}(-1)^{j+1}\left(\frac{j\pi x}{\ell}\right)^2, \qquad \gamma_j(x) = \phi_j(x) + x^j + 1 \tag{6}$$

The array deflection and distributed moment are then:

$$\xi(x,t) = \boldsymbol{\phi}(x)^T\boldsymbol{\eta}(t), \qquad M(x,t) = \boldsymbol{\gamma}(x)^T\boldsymbol{q}(t) \tag{7}$$

For the co-design studies, 4 approximating functions are used. This approximation parameterizes the control as a spatially-varying distributed moment but the control input on a piezoelectric segment is typically a uniform voltage.[51] Comparing both of these representations in Figs. 2a and 2b, we may think of the spatially-varying distributed moment as the limiting case of the piecewise uniform moment. The applicability of this approximation to a real implementable physical system will be discussed later.

Now we want to derive a system of ordinary differential equations (ODEs) that approximate the PDE given above. The discretization is done by minimizing weighted residual of the ξ dynamics. Using the above

formulation and defining following term matrices we obtain:

$$[\boldsymbol{M_g}]\begin{bmatrix}\ddot{\theta}\\ \ddot{\boldsymbol{\eta}}\end{bmatrix}+[\boldsymbol{C_g}]\begin{bmatrix}\dot{\theta}\\ \dot{\boldsymbol{\eta}}\end{bmatrix}+\begin{bmatrix}0\\ 2[\boldsymbol{e}](\boldsymbol{\eta}+\mu\dot{\boldsymbol{\eta}})\end{bmatrix}=\begin{bmatrix}d\\ \int_0^\ell 2\boldsymbol{\phi}M^{''}dx\end{bmatrix} \tag{8}$$

$$\text{where:}\qquad [\boldsymbol{M_g}]=\begin{bmatrix}\left(J_\theta+2\int_0^\ell m_R\left(x+r\right)^2dx+2\boldsymbol{\eta}^T\left([\boldsymbol{A}]-[\boldsymbol{B}]\right)\boldsymbol{\eta}\right) & 2[\boldsymbol{C}]\\ 2[\boldsymbol{C}]^T & 2[\boldsymbol{A}]\end{bmatrix}$$

$$[\boldsymbol{C_g}]=\begin{bmatrix}2\dot{\boldsymbol{\eta}}^T\left([\boldsymbol{A}]-[\boldsymbol{B}]\right)\boldsymbol{\eta} & 2\boldsymbol{\eta}^T\left([\boldsymbol{A}]-[\boldsymbol{B}]\right)\dot{\theta}\\ -2([\boldsymbol{A}]-[\boldsymbol{B}])\boldsymbol{\eta}\dot{\theta} & 0\end{bmatrix}$$

$$[\boldsymbol{A}]=\int_0^\ell m_R\boldsymbol{\phi}\boldsymbol{\phi}^Tdx,\qquad [\boldsymbol{B}]=\int_0^\ell p\boldsymbol{\phi}^{'}\boldsymbol{\phi}^{'T}dx,\qquad [\boldsymbol{C}]=\int_0^\ell m_R(x+r)\boldsymbol{\phi}^Tdx$$

$$[\boldsymbol{D}]=-[\boldsymbol{B}],\qquad [\boldsymbol{e}]=(EI)^{'}(\ell)\boldsymbol{\phi}(\ell)\boldsymbol{\phi}^{''T}(\ell)-EI(\ell)\boldsymbol{\phi}^{'}(\ell)\boldsymbol{\phi}^{''T}(\ell)+\int_0^\ell EI\boldsymbol{\phi}^{''}\boldsymbol{\phi}^{''T}dx$$

The boundary conditions with the approximating functions are then:

$$\boldsymbol{\phi}(0)^T=\boldsymbol{\phi}^{'}(0)^T=0,\quad EI\boldsymbol{\phi}^{''}(\ell)^T\left(\boldsymbol{\eta}+\mu\dot{\boldsymbol{\eta}}\right)=M(x,t)\Big|_{x=\ell},\quad EI\boldsymbol{\phi}^{'''}(\ell)^T\left(\boldsymbol{\eta}+\mu\dot{\boldsymbol{\eta}}\right)=M^{'}(x,t)\Big|_{x=\ell} \tag{9}$$

II.A.3. Structural Model

The structural geometry of the array is also designed simultaneously with the distributed moment. In this work, the length of the array and the distributed thickness are optimized. In order to implement the distributed thickness, the length of the array is divided into multiple segments as shown in Fig. 2c. The absolute locations of the segment boundaries is represented by a parameter vector $\boldsymbol{\ell}$, and the thickness on the segment boundaries is represented by a parameter vector $\boldsymbol{h}$. On segment j, the thickness varies linearly with respect to x as:

$$h_j(x)=(h_{j+1}-h_j)\frac{x-\ell_j}{\ell_{j+1}-\ell_j}+h_j,\qquad x\in[\ell_j,\ell_{j+1}] \tag{10}$$

Letting a subscript $(\cdot)_1$ refer to the original array properties and $(\cdot)_2$ to the piezoelectric layer properties, the total flexural rigidity is given by $EI(x)=E_1I_1(x)+E_2I_2(x)$, and the total mass per unit length is $m_R(x)=m_{R1}(x)+m_{R2}(x)$. It is also assumed that the entire top surface of the array is covered with piezoelectric material of thickness constant h_2.

II.B. Pseudo-Rigid Body Dynamic Model

A PRBDM was developed for the spacecraft system for the purpose of performing additional numerical studies that complement those based on the PDE model, including studies that yield qualitative insights that are difficult to obtain via the more sophisticated PDE model. The flexible solar arrays were modeled both with single and multi-link approximations. The single link model is presented here, where each array is modeled as a single rigid link connected to the spacecraft body via a revolute joint and a torsional spring. This is a lumped compliance approximation of the distributed compliance of the actual solar array.

Figure 1b illustrates this single-link system model with three total rigid members: two solar arrays and the spacecraft body. Internal moments are applied at the revolute joints, and both arrays undergo the same moment M to produce spacecraft body rotations. A PRBDM links the motion and force of an elastic member and a rigid-body mechanism through a set of diagrams and equations that describe this correspondence.[37] The foundation of this theory is the principle of dynamic equivalence.[52] The main advantage of PRBDMs is a computational favorable, accurate simplification of large-deflection nonlinear analysis of beams.[37] However, these models only describe the behavior at a component level rather than the specific point-to-point variations while Euler-Bernoulli beam in Sec. II.A does capture these variations. In addition, the lumped parameters required in the PRBDM must be chosen carefully to accurately model the system and currently there is no direct mapping from the beam geometric properties to the lumped parameters such as stiffness and damping. However, reasonable approximations for the lumped parameters can be utilized and important qualitative insights can be gained from this type of model.

Applying the Euler-Lagrange equation to the system in Fig. 1b we arrive at the following equations of motion:

$$\mathcal{M}\begin{bmatrix}\ddot{\theta}\\ \ddot{\delta}\end{bmatrix}+\mathcal{B}\begin{bmatrix}\dot{\theta}\\ \dot{\delta}\end{bmatrix}+\mathcal{K}\begin{bmatrix}\theta\\ \delta\end{bmatrix}=\boldsymbol{\tau} \tag{11}$$

$$\text{where:}\qquad \mathcal{M}=\begin{bmatrix}J_\theta+2J_\delta+2mr^2+\frac{1}{2}m\ell^2+2\ell mr\cos(\delta) & 2J_\delta+mr\ell\cos(\delta)+\frac{1}{2}m\ell^2\\ 2J_\delta+mr\ell\cos(\delta)+\frac{1}{2}m\ell^2 & 2J_\delta+\frac{1}{2}m\ell^2\end{bmatrix}$$

$$\mathcal{B}=\begin{bmatrix}-2\ell mr\dot{\delta}\sin(\delta) & -\ell mr\dot{\delta}\sin(\delta)\\ \ell mr\dot{\theta}\sin(\delta) & 2b\end{bmatrix},\qquad \mathcal{K}=\begin{bmatrix}0 & 0\\ 0 & 2k\end{bmatrix},\qquad \boldsymbol{\tau}=\begin{bmatrix}q\\ 2M\end{bmatrix}$$

$$m=\rho\ell wh,\qquad J_\delta=\frac{1}{12}m\left(\ell^2+h^2\right)$$

where k is the torsional spring stiffness at the revolute joints. Solving the eigenvalue problem ($\mathcal{M}^{-1}\mathcal{K}=\boldsymbol{\omega}^2$) gives the natural frequencies of the system:

$$\omega_1^2=0 \tag{12a}$$

$$\omega_2^2=k\frac{2m\ell^2+8m\ell r\cos(\delta)+8mr^2+4J_\theta+8J_\delta}{-2\ell^2m^2r^2\cos(\delta)^2+2\ell^2m^2r^2+J_\theta\ell^2m+8J_\delta mr^2+4J_\theta J_\delta}=\frac{k}{J_{\text{eff}}(\delta,\ell,h,w)} \tag{12b}$$

One of the eigenfrequencies is zero since the system permits a rigid body mode. The two mode shapes are:

$$\boldsymbol{\Psi}=\begin{bmatrix}\boldsymbol{\psi}_1 & \boldsymbol{\psi}_2\end{bmatrix}=\begin{bmatrix}1 & -\frac{m\ell^2+2mr\ell\cos(\delta)+4J_\delta}{m\ell^2+4mr\ell\cos(\delta)+4mr^2+2J_\theta+4J_\delta}\\ 0 & 1\end{bmatrix} \tag{13}$$

We note that the nonrigid mode eigenfrequency (ω_2) and eigenvector ($\boldsymbol{\psi}_2$) are not constant but depend on the path of the array. The total angular momentum of the system is:

$$\mu=\left(\frac{1}{2}\ell^2m+2\ell mr\cos(\delta)+2mr^2+J_\theta+2J_\delta\right)\dot{\theta}+\left(\frac{1}{2}\ell^2m+\ell mr\cos(\delta)+2J_\delta\right)\dot{\delta} \tag{14}$$

Since internal moments cannot change the total angular momentum of the system, the only mode that is present in the absence of external moments is the momentum conserving mode $\boldsymbol{\psi}_2$.

III. Co-Design Problem Formulation

The objective of the co-design study is to provide insights into how the physical solar array should be designed to optimize the performance of the actively controlled array with respect to pointing and jitter reduction. A balanced co-design approach is utilized where physical design is considered in a comprehensive manner.[25] A general simultaneous co-design formulation (with a fixed time horizon) is:

$$\min_{\boldsymbol{x}_c,\boldsymbol{x}_p}\quad J(t,\boldsymbol{\xi},\boldsymbol{x}_c,\boldsymbol{x}_p) \tag{15a}$$

$$\text{subject to:}\quad \dot{\boldsymbol{\xi}}(t)-\boldsymbol{f}(t,\boldsymbol{\xi},\boldsymbol{x}_c,\boldsymbol{x}_p)=\mathbf{0} \tag{15b}$$

$$\boldsymbol{c}(t,\boldsymbol{\xi},\boldsymbol{x}_c,\boldsymbol{x}_p)\leq\mathbf{0} \tag{15c}$$

$$\boldsymbol{c}_{\text{eq}}(t,\boldsymbol{\xi},\boldsymbol{x}_c,\boldsymbol{x}_p)=\mathbf{0} \tag{15d}$$

where $\boldsymbol{x}_c$ are the control design variables, $\boldsymbol{x}_p$ are the physical system design variables, and $\boldsymbol{\xi}$ are the states, Eq. (15a) is a general performance objective, Eq. (15b) enforces the feasible dynamics, Eq. (15c) are general inequality constraints, and Eq. (15d) are general equality constraints. Here the physical system design is parameterized by $\boldsymbol{h}$ and $\boldsymbol{\ell}$ with 10 distinct linear segments. The control system design is defined by $\boldsymbol{q}(t)$ which are used to compute $M(x,t)$.

The task is divided into two phases where $\bar{t}$ denotes the time dividing the phases. The first phase concentrates on rotating the bus from a specific angular displacement, i.e., slewing. The second phase consists of maintaining the bus inertially fixed to a given tolerance for precision pointing. The objective

Table 1: Bus parameters.

J_θ	372.49 kg m^2
r	1.02 m

Table 2: Array parameters.

ℓ_{nominal}	1.575 m	E_1	1.57 GPa	E_2	62 GPa
h_{nominal}	0.018 m	ρ_1	332.03 kg/m^3	ρ_2	7800 kg/m^3
w_{nominal}	1.862 m	μ	10^{-4}	h_2	10^{-3} m

function to minimize is the damping error in the pointing phase since instruments such as mirrors cannot manage high frequency vibration:

$$J = \int_{\bar{t}}^{t_f} \dot{\theta}^2 dt \tag{16a}$$

where $t \in [t_0, t_f] = [0 \text{ s}, 2 \text{ s}]$ and $\bar{t} = 1$ s. The dynamic constraint uses the ODE defined in Eq. (8) with 4 approximating functions. The physical parameters for the bus, array, and piezoelectric layer are shown in Tables 1 and 2. A disturbance moment $d(t)$ on the bus is present during the slewing and pointing phases. It consists of a jitter component (e.g., vibration from reaction wheels, pumps) and a bias component (e.g., solar radiation pressure, atmospheric drag):

$$d(t) = 10^{-4} \text{ Nm} + 2 \times 10^{-3} \sin(50t) \text{ Nm} \tag{16b}$$

The initial configuration is stationary with a constant offset to θ denoted θ_0 so the initial states are constrained to be:

$$\begin{bmatrix} \theta \\ \dot{\theta} \\ \boldsymbol{\eta} \\ \dot{\boldsymbol{\eta}} \end{bmatrix}_{t=t_0} = \begin{bmatrix} \theta_0 \\ 0 \\ \mathbf{0} \\ \mathbf{0} \end{bmatrix} \tag{16c}$$

The bus angle is constrained to zero during the pointing phase. A tolerance value is defined because pointing control of instruments such as mirrors can correct for small angular offsets:

$$|\theta(t)| \leq 10^{-5}, \qquad t \in [\bar{t}, t_f] \tag{16d}$$

PEMA actuation magnitude is also limited based on their physical properties and maximum voltage restrictions:

$$|M(x,t)| \leq 20 \text{ Nm/m} \tag{16e}$$

The strain $\epsilon(x,t)$ on the array surface is constrained to maintain structural integrity and to avoid undesirable dynamic effects:

$$|\epsilon(x,t)| = \left| \frac{h(x)}{2} \xi'' \right| \leq 10^{-4} \tag{16f}$$

The array length ℓ_{10} and the dimensions of the linear array elements have manufacturing and operational constraints:

$$\begin{aligned} 0.5 \text{ m} \leq l_{10} \leq 2.5 \text{ m} \\ 0.05 \text{ m} \leq l_{i+1} - l_i \leq 2.5 \text{ m} \qquad i = 0, 1, \ldots, 10 \\ 0.009 \text{ m} \leq h_i \leq 0.028 \text{ m} \end{aligned} \tag{16g}$$

The array volume is constrained to the nominal value in order to avoid increasing the payload mass and delivery costs. This is proportional to the array structure cross-sectional area:

$$\sum_{i=1}^{10} \frac{w}{2}(h_{i-1}+h_i)(l_i-l_{i-1}) = 0.054 \text{ m}^3 \tag{16h}$$

The array planform area is constrained to the nominal value to maintain the same level of power generation:

$$l_{10}w = 2.932 \text{ m}^2 \tag{16i}$$

This completes the co-design problem formulation. The results for a number of minor variations on this formulation will be discussed next after a short study on the fundamental limits of a slewing maneuver with SASA.

IV. Analytical and Numerical Results for SASA System

IV.A. Maximum Slewing Bounds using the PRBDM

The momentum of the PRBDM system is given in Eq. (14) and it must be conserved if there is no external disturbance on the bus ($d \equiv 0$). Assuming zero initial momentum, we can integrate the momentum equation to determine the relationship between θ and δ:

$$\begin{aligned} 0 &= \left(\frac{1}{2}\ell^2 m + 2\ell m r\cos(\delta) + 2mr^2 + I_\theta + 2I_\delta\right)\dot{\theta} + \left(\frac{1}{2}\ell^2 m + \ell m r\cos(\delta) + 2I_\delta\right)\dot{\delta} \\ &:= I_1(\ell,h,w,\delta)\dot{\theta} + I_2(\ell,h,w,\delta)\dot{\delta} \\ \dot{\theta} &= -\frac{I_2(\delta,\cdot)}{I_1(\delta,\cdot)}\dot{\delta} \\ \theta(t_f) - \theta(t_0) &= -\int_{t_0}^{t_f} \frac{I_2(\delta,\cdot)}{I_1(\delta,\cdot)}\dot{\delta}dt \end{aligned} \tag{17}$$

The question we are trying to answer requires an upper bound on $|\theta(t_f)|$. We can find a reasonable upper bound by determining the maximum value of the integrals. Recall that m and I_δ are dependent on the geometric physical design variables. Since the geometric variables are positive and it is reasonable to assume $\cos(\delta) > 0$ (panel angle must be smaller than $|\delta| < \pi/2$), then we see that both α and β are strictly positive since they are the sum of positive products:

$$\begin{aligned} 0 < \alpha \qquad &\text{where: } \alpha(\ell,h,w,\delta) = \frac{1}{2}\ell^2(\rho\ell wh) + \ell(\rho\ell wh)r\cos(\delta) + 2\left(\frac{1}{12}m\left(\ell^2+h^2\right)\right) \\ 0 < \beta \qquad &\text{where: } \beta(\ell,h,w,\delta) = \ell(\rho\ell wh)r\cos(\delta) + 2(\rho\ell wh)r^2 + I_\theta \end{aligned}$$

Therefore the effective inertia ratio must be between 0 and 1:

$$\begin{aligned} \frac{I_2}{I_1} &= \frac{\alpha}{\alpha+\beta} \\ \inf_{\alpha>0,\beta>0}\left(\frac{\alpha}{\alpha+\beta}\right) &= \lim_{\beta\to\infty}\left(\frac{\alpha}{\alpha+\beta}\right) = 0, \qquad \sup_{\alpha>0,\beta>0}\left(\frac{\alpha}{\alpha+\beta}\right) = \lim_{\alpha\to\infty}\left(\frac{\alpha}{\alpha+\beta}\right) = 1 \end{aligned} \tag{18}$$

If $|\delta(t)| \le \delta_{\max}$ is small, then the effective inertia ratio is nearly time-independent. Therefore we can choose the effective inertia ratio as its largest potential value to arrive at the following inequality:

$$\begin{aligned} |\theta(t_f) - \theta(t_0)| &\le \left|-\int_{t_0}^{t_f}\dot{\delta}dt\right| \\ &\le |\delta(t_0) - \delta(t_f)| \end{aligned} \tag{19}$$

Assuming $\delta(t_0) = 0$, $\theta(t_f) = 0$, and we hit the prescribed bound on δ at t_f, then we have:

$$|\theta_0| \le \delta_{\max} \tag{20}$$

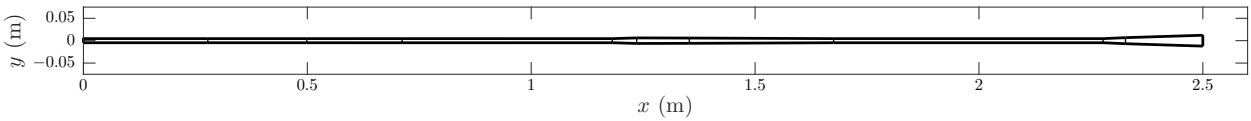

(a) Array shape (drawn to scale).

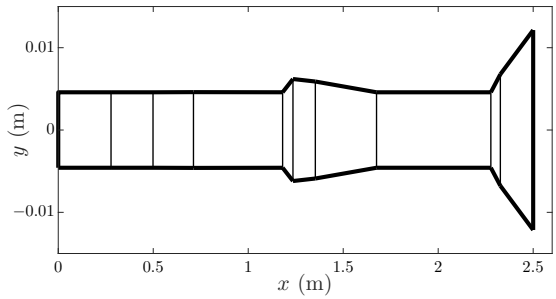

(b) Array shape (not drawn to scale).

Figure 3: Optimal array shape for $\theta_0 = 3$ mrad and reduced mass of 9.96 kg.

Therefore we expect the maximum change for the bus angle to be upper bounded by the allowable change in panel angle using only internal actuation of the solar panel. This implies that if only milli-radian deflections of the array are feasible, we can only achieve, at most, milli-radian changes in the pointing accuracy of the bus. An comparable $\delta_{\max}$ condition for a continuous beam is a strain bound. Additional novel solutions for SASA such as revolute joints that allow for large changes in the effective inertia ratio without violating conservation of momentum may extend this limit.

IV.B. Co-design Studies

Here we study three variations on the co-design problem introduced in Sec. III: nominal geometry (NG), variable length (VL), and piecewise linear segments (PLS). The nominal array geometry is presented in Table 2. The VL case has only ℓ as the unique physical-system design variable (see Fig. 2a), and the PLS case varies both array length and thickness to perform distributed geometric design of the structure (see Fig. 2c). Several slew angles between 1 mrad and 3 mrad were used to investigate the slewing limits and its effect on the optimal design. Here all solutions are found using the $\mathbb{GPOPS}-\mathbb{II}$ software package for MATLAB, which uses a pseudospectral method with Legendre-Gauss-Radau (LGR) collocation points and an *hp*-adaptive mesh refinement algorithm.[53]

The parametric study with nominal array mass yielded results for the PLS and VL cases for slew magnitudes less or equal than 2 mrad; convergence became much slower for larger slew magnitudes due to difficulties in satisfying the strain constraints. Furthermore, the strain constraints made the NG case infeasible for all the tested slew magnitudes. These results indicate that the performance level desired may not be achievable through control design alone, and that there is a limit on the maximum achievable slewing angle. Observations of the strain profile show that the limit in Eq. (16f) is active or nearly active in many of the cases (see Figs. 8 and 9). We investigated the strain required to achieve the desired slewing performance for the NG case by minimizing the maximum array strain, and discovered that the resulting strain values were larger than the constraint tolerance. Adding degrees of freedom to the structural design problem allows achieving higher performance levels through synergistic structural tailoring. These results agree with the findings on slewing limits presented in Sec. IV.A.

Although the main parametric study considers the array mass to be constant and nominal ($m = 17.85$ kg), additional simulations were conducted to investigate feasibility with reduced array mass. This only considers the mass of the base array since the piezoelectric layer is present in all cases and covers the entire array area with a mass of 22.87 kg, approximately. The best array design found that achieves the largest slew maneuver with minimum array mass ($\theta_0 = 3$ mrad and $m = 9.96$ kg for the PLS case) is shown in Fig. 3 (in Fig. 3b, the thickness is magnified to show the profile changes clearly). The respective bus angle and angular rate histories are shown in Fig. 4.

The results of the parametric study show that in addition to satisfying the prescribed slew and pointing

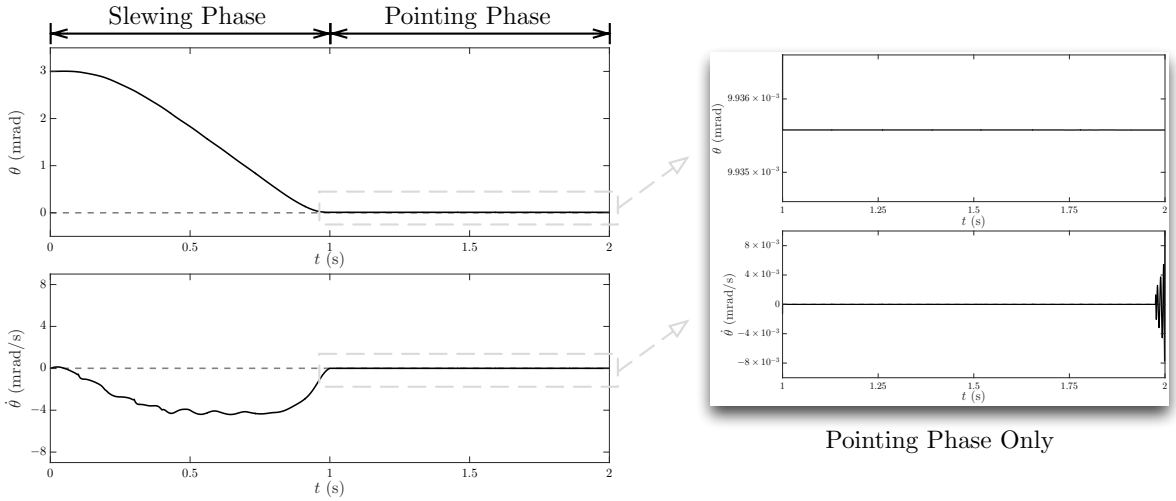

Figure 4: Bus angle and velocity trajectories for $\theta_0 = 3$ mrad with piecewise linear segments (PLS) and reduced array mass of 9.96 kg.

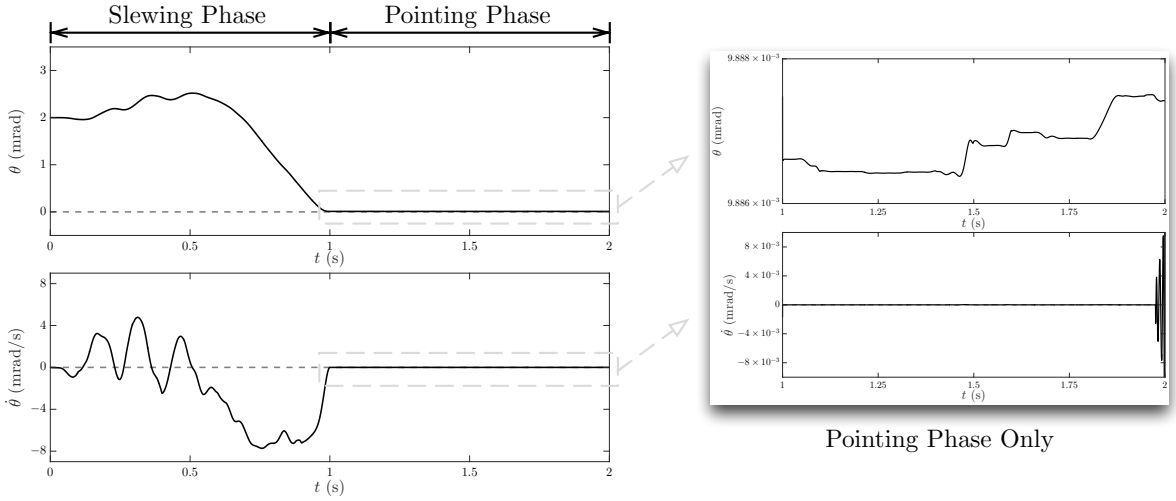

Figure 5: Bus angle and velocity trajectories for $\theta_0 = 2$ mrad with variable length (VL) and nominal mass.

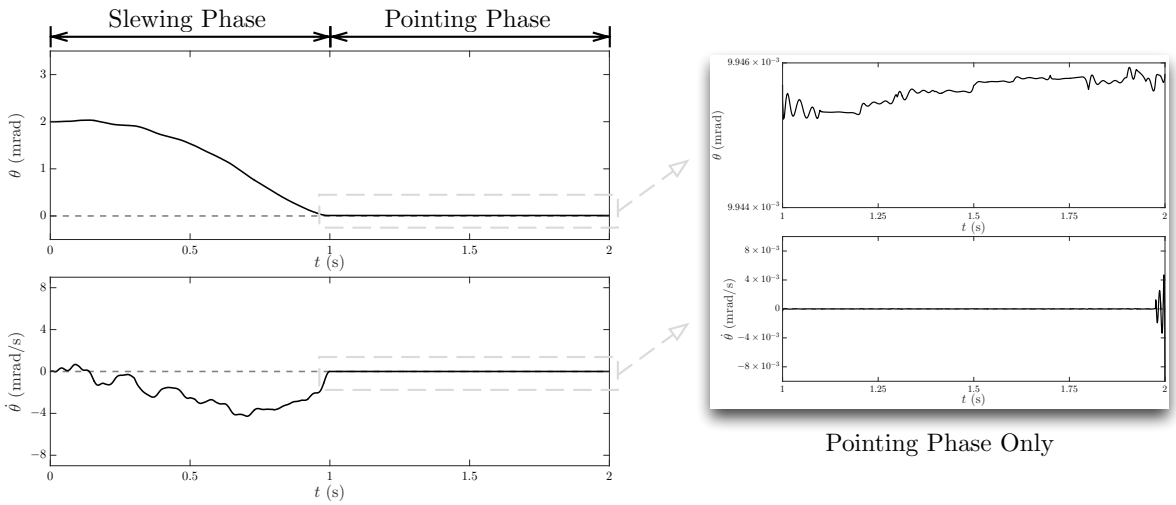

Figure 6: Bus angle and velocity trajectories for $\theta_0 = 2$ mrad with piecewise linear segments (PLS) and nominal mass.

maneuvers, the main driver in the design optimization is the satisfaction of the strain constraints. This is accomplished by increasing the moment of inertia of the array or by reducing the array thickness in locations of high curvature, which act like joints. A distributed thickness design also allows to tailor array modes for optimal active dynamic performance. The optimal histories for the bus angle and angular rate for a slew maneuver of 2 mrad for the VL and PLS cases are shown in Figs. 5 and 6, respectively.

The array deflections for the parametric study are shown in Figs. 10 and 11 for both VL and PLS design cases where the array mass is nominal; results from slewing and pointing phases are shown separately. Conservation of angular momentum in the bus-array system provides an explanation of the observations from the numerical simulations:

- Rotating the bus CW requires the array to displace in the opposite direction (CCW) (see Fig. 1a).
- Larger slew maneuvers require larger array displacements (see Sec. IV.A).

Figure 7 shows the design evolution of the VL and PLS cases with respect to the magnitude of the slew maneuver. All the VL cases tend towards the maximum allowable array length since this design maximizes the moment of inertia, which helps reduce the strain. In the PLS cases, the design trend of increasing the moment of inertia is similar up to the slew magnitude of 1.5 mrad, where the design trend switches to control the strain by defining several locations of small thickness. Ongoing work includes modal analysis and other studies with the objective of explaining why these more complex cases perform better. Higher spatial resolution in the structural design representation will provide refined results that, along with deeper analysis of these designs and tradeoffs, may lead to explanatory design theories for integrated design of distributed actuation and distributed structural shape design problems.

Figures 8 and 9 show the strain history of the array for the studied cases. It is shown that in most cases, the array has 2 locations of high strain and 3 locations of low strain (2 locations for the 2 mrad slew maneuver in the PLS case). This indicates that a PRBDM with 2 joints and 3 rigid links may approximate the optimal dynamic behavior of the flexible array with similar mode shapes. The optimal distributed deflection behavior is achieved in both design cases, i.e VL and PLS cases, but through different means. In the VL case, the optimal deflection time history is achieved through the distributed control profile as shown in Fig. 12. In the PLS case, the optimal deflection behavior is achieved by the combined design of the distributed control profile and the distributed array geometry (see Figs. 13 and 7). The presence of an effective "joint" or "link" at a particular location depends on the local thickness and the moment magnitude at that location. Such a combined effect allows the distributed moment profiles to be more simple and uniform for the PLS case, and help achieve superior jitter reduction in the pointing phase compared to the VL case as shown in the array deflection profiles in Figs. 10–11.

The application of a continuously variable distributed moment is not a physically realizable actuation strategy, but the optimal results of this co-design problem can provide insights into performance limits and how a physically realizable strain actuation system should be designed. Continuous moment variation can be approximated using several piezoelectric segments as shown in Fig. 2b where a constant voltage $V_i(t)$ is applied to each of segment. A co-design problem based on segmented strain actuators would produce designs that are closer to implementable, where the optimization problem identifies the segment voltage trajectories, distributed beam thickness, and segment lengths that together produce optimal system performance. Ongoing work involves co-design studies based on segmented strain actuators, including physical prototyping and lab-scale testing of a representative SASA system with digital feedback control.

V. Conclusions

In this work we investigated the integrated structural and control-system design of a strain-actuated solar array for spacecraft pointing control and jitter reduction. Slew maneuvers on the order of milli-radians have been achieved in simulations for a representative spacecraft system without increasing the total array mass or reducing the array area. A parametric study was conducted with different design cases and multiple slew magnitudes while maintaining the nominal array mass. Results show that only designing the control system may not achieve the desired performance, but the combined design of the structures and control systems can help achieve better performance. Furthermore, adding degrees of freedom to the structural design—specifically, distributed geometric design—improved performance further.

Since the SASA system is based on internal actuation, the angular momentum of the bus-array system must be conserved. A desired bus rotation requires array deflection in the opposite direction. Results

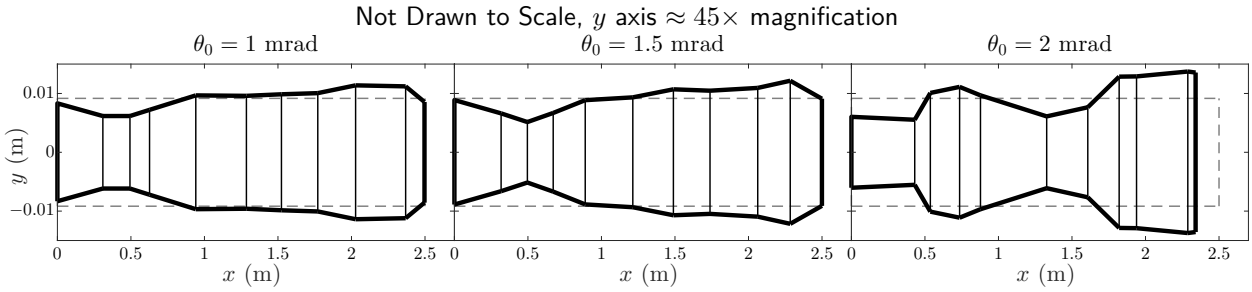

Figure 7: Array shapes for both variable length (dashed) and piecewise linear segments (solid) studies (nominal mass constraint).

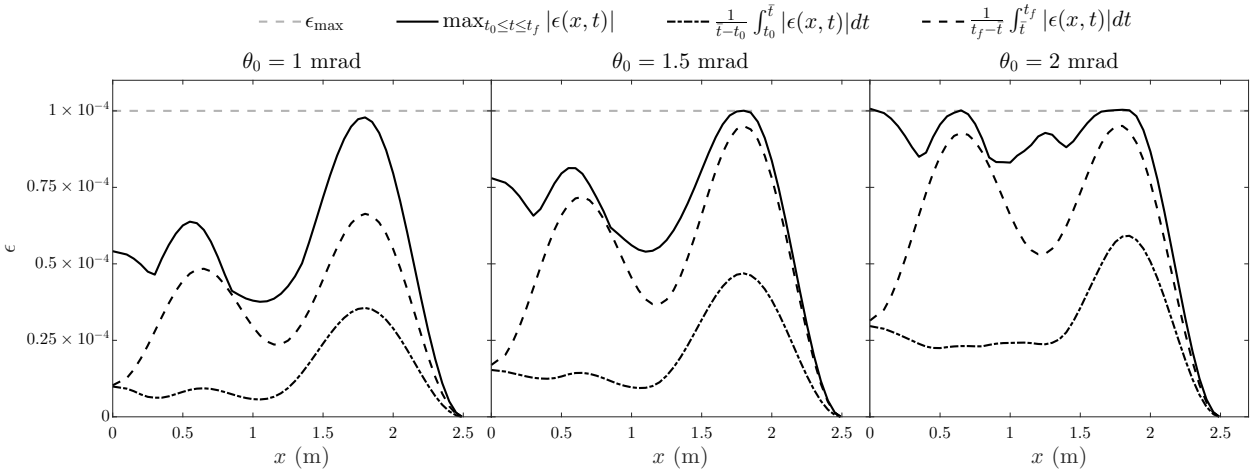

Figure 8: Strain metrics for select values of θ_0 with variable length (VL) and nominal mass.

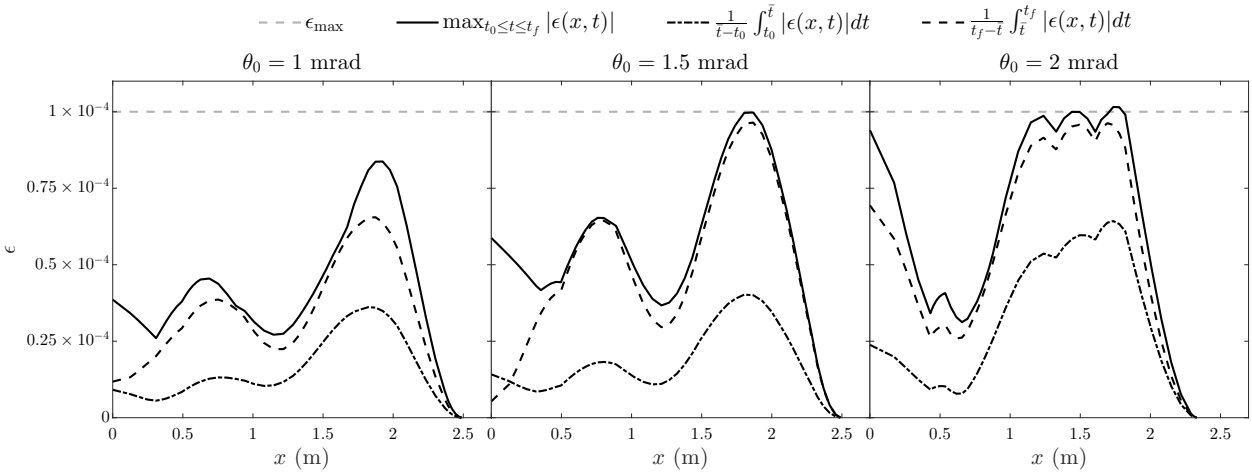

Figure 9: Strain metrics for select values of θ_0 with piecewise linear segments (PLS) and nominal mass.

showed that in addition to accomplishing the required slewing and pointing maneuvers, the array design is also driven by the strain constraint. This constraint can be satisfied by increasing the moment of inertia of the array or by defining array locations of small thickness for high strain. The latter strategy, available only in the PLS case, yields complex distributed shape designs that may be desirable for producing modes that support optimal active performance. A second investigation on the minimum array mass yielded the best design found that maximizes the slew magnitude and shows the benefits of using a thin array of high density material to control the strain and to provide enough moment of inertia for the maneuvers. Maximum bus slew limits achievable through SASA control were investigated using PRBDM analysis. At best a unitary ratio of bus to array rotation can be achieved using this initial SASA architecture.

Results also show that the dynamic behavior of the array may be approximated by a PRBDM system with rigid links and joints. This connection may help provide qualitative insights into the design and behavior of distributed geometry intelligent structures. Virtual joints and links can be identified in the numerical results. In the constant thickness cases 'joints' are evident when localized internal moments are high. The same effect can be achieved more effectively through a combination of large localized moments and designing thinner portions of the array geometry. When both spatially distributed moments and distributed structural shape design are employed simultaneously, improved jitter reduction and smoother control profiles result.

Future work includes deeper analysis of resulting optimal designs and identification of design principles for integrated design of intelligent structures with distributed geometric design flexibility. Additional future studies will concentrate on more complex pointing maneuvers, three-axis rotation studies, new models (e.g., including array torsion and tension), and new SASA architectures (e.g., incorporation of revolute/gimbaled joints) that support a wider range of slew maneuvers, including large multi-axis reorientations.

Acknowledgments

Government sponsorship is acknowledged. The research was in part carried out at the Jet Propulsion Laboratory, California Institute of Technology under a contract with the National Aeronautics and Space Administration. The authors acknowledge help from Giri Subramanian and Kevin Lohan during the initial phases of the project.

References

[1]Arnon, S., Rotman, S., and Kopeika, N. S., "Optimum Transmitter Optics Aperture for Satellite Optical Communication," *IEEE Transactions on Aerospace and Electronic Systems*, Vol. 34, No. 2, Aug. 1998, pp. 590–596, doi: 10.1109/7.670339

[2]Ruiter, A. F. D., Damaren, C., and Forbes, J. R., *Spacecraft Dynamics and Control: An Introduction*, John Wiley & Sons, 2013.

[3]Sirlin, S. W., "Vibration Isolation for Spacecraft Using the Piezoelectric Polymer PVF2," *Journal of the Acoustical Society of America*, Vol. 82, No. S13, Nov. 1987, doi: 10.1121/1.2024666

[4]Rao, S. S. and Sunar, M., "Piezoelectricity and Its Use in Disturbance Sensing and Control of Flexible Structures: A Survey," *Applied Mechanics Reviews*, Vol. 47, No. 4, April 1994, pp. 113–123, doi: 10.1115/1.3111074

[5]Cowen, R., "The Wheels Come Off Kepler," *Nature*, Vol. 497, No. 7450, 2013, pp. 417–418, doi: 10.1038/497417a

[6]Coverstone-Carroll, V. L. and Wilkey, N. M., "Optimal Control of a Satellite-Robot System Using Direct Collocation with Non-linear Programming," *Acta Astronautica*, Vol. 36, No. 3, Aug. 1995, pp. 149–162, doi: 10.1016/0094-5765(95)00096-I

[7]Meckl, P. H. and Kinceler, R., "Robust Motion Control of Flexible Systems Using Feedfoward Forcing Functions." *IEEE Transactions on Control Systems Technology*, Vol. 2, No. 3, Sept. 1994, pp. 245–254, doi: 10.1109/87.317981

[8]Manning, R. A., "Optimum Design of Intelligent Truss Structures," *32nd Structures, Structural Dynamics, and Materials Conference*, Baltimore, MA, USA, April 1991, pp. 528–533, doi: 10.2514/6.1991-1158

[9]Smith, M. J., Grigoriadis, K. M., and Skelton, R. E., "Optimal Mix of Passive and Active Control in Structures," *Journal of Guidance, Control, and Dynamics*, Vol. 15, No. 4, July–Aug. 1992, pp. 912–919, doi: 10.2514/3.20924

[10]Meirovitch, L., *Dynamics and Control of Structures*, John Wiley & Sons, 1990.

[11]Crawley, E. F. and Luis, J. D., "Use of Piezoelectric Actuators as Elements of Intelligent Structures," *AIAA Journal*, Vol. 25, No. 10, Oct. 1987, pp. 1373–1385, doi: 10.2514/3.9792

[12]Wada, B. K., Fanson, J. L., and Crawley, E. F., "Adaptive Structures," *Journal of Intelligent Material Systems and Structures*, Vol. 1, No. 2, April 1990, pp. 157–174, doi: 10.1177/1045389X9000100202

[13]Balas, M. J., "Active Control of Flexible Systems," *Journal of Optimization Theory and Applications*, Vol. 25, No. 3, July 1978, pp. 415–436, doi: 10.1007/BF00932903

[14]Bailey, T. and Hubbard Jr., J. E., "Distributed Piezoelectric-Polymer Active Vibration Control of a Cantilever Beam," *Journal of Guidance, Control, and Dynamics*, Vol. 8, No. 5, Sept. 1985, pp. 605–611, doi: 10.2514/3.20029

[15]Fanson, J. L. and Chen, J. C., "Structural Control by the Use of Piezoelectric Active Members," *NASA-Langley Research Center NASA/DOD Control/Structures Interaction Technology*, 1986, pp. 809–829.

[16]Pan, J., Hansen, C. H., and Snyder, S. D., "A Study of the Response of a Simply Supported Beam to Excitation by a Piezoelectric Actuator," *Journal of Intelligent Material Systems and Structures*, Vol. 3, No. 1, Jan. 1992, pp. 3–16, doi: 10.1177/1045389X9200300101

[17]Hubbard Jr., J. E. and Burke, S. E., "Distributed Transducer Design for Intelligent Structural Components," *Intelligent Structural Systems*, edited by H. S. Tzou and G. L. Anderson, Vol. 13, Springer, 1992, pp. 305–324, doi: 10.1007/978-94-017-1903-2_8

[18]Hwang, W. and Park, H. C., "Finite Element Modeling of Piezoelectric Sensors and Actuators," *AIAA Journal*, Vol. 31, No. 5, May 1993, pp. 930–937, doi: 10.2514/3.11707

[19]Alvarez-Salazar, O. S. and Iliff, K., "Destabilizing Effects of Rate Feedback on Strain Actuated Beams," *Journal of Sound and Vibration*, Vol. 221, No. 2, March 1999, pp. 289–307, doi: 10.1006/jsvi.1998.2010

[20]Dimitriadis, E. K., Fuller, C. R., and Rogers, C. A., "Piezoelectric Actuators for Distributed Vibration Excitation of Thin Plates," *Journal of Vibration and Acoustics*, Vol. 113, No. 1, Jan. 1991, pp. 100–107, doi: 10.1115/1.2930143

[21]Pinkerton, J. L., McGowan, A.-A. R., Moses, R. W., Scott, R. C., , and Heeg, J., "Controlled Aeroelastic Response and Airfoil Shaping Using Adaptive Materials and Integrated Systems," *Symposium on Smart Structures and Materials*, San Diego, CA, USA, Feb. 1996, pp. 166–177.

[22]Fowler, R. M., *Investigation of Compliant Space Mechanisms with Application to the Design of a Large-Displacement Monolithic Compliant Rotational Hinge*, M.S. Thesis, Brigham Young University, Aug. 2012.

[23]Junkins, J. L. and Rew, D. W., "Unified Optimization of Structures and Controllers," *Large Space Structures: Dynamics and Control*, edited by S. N. Atluri and A. K. Amos, Springer Series in Computational Mechanics, Springer, 1988, pp. 323–353, doi: 10.1007/978-3-642-83376-2_14

[24]Allison, J. T., Guo, T., and Han, Z., "Co-Design of an Active Suspension Using Simultaneous Dynamic Optimization," *Journal of Mechanical Design*, Vol. 136, No. 8, Aug. 2014, pp. 081003, doi: 10.1115/1.4027335

[25]Allison, J. T. and Herber, D. R., "Multidisciplinary Design Optimization of Dynamic Engineering Systems," *AIAA Journal*, Vol. 52, No. 4, April 2014, pp. 691–710, doi: 10.2514/1.J052182

[26]Salama, M., Garba, J., and Demsetz, L., "Simultaneous Optimization of Controlled Structures," *Computational Mechanics*, Vol. 3, No. 4, July 1988, pp. 275–282, doi: 10.1007/BF00368961

[27]Wu, Z., Harne, R. L., and Wang, K.-W., "Energy Harvester Synthesis Via Coupled Linear-Bistable System with Multistable Dynamics," *Journal of Applied Mechanics*, Vol. 81, No. 6, Feb. 2014, pp. 061005, doi: 10.1115/1.4026555

[28]Grigoriadis, K. M., Zhu, G., and Skelton, R. E., "Optimal Redesign of Linear Systems," *Journal of Dynamic Systems, Measurement, and Control*, Vol. 118, No. 3, Sept. 1993, pp. 598–605, doi: 10.1115/1.2801186

[29]Allison, J. T., Kokkolaras, M., and Papalambros, P. Y., "On Selecting Single-Level Formulations for Complex System Design Optimization," *Journal of Mechanical Design*, Vol. 129, No. 9, Sept. 2006, pp. 898–906, doi: 10.1115/1.2747632

[30]Fanson, J. L. and Caughey, T. K., "Positive Position Feedback Control for Large Space Structures," *AIAA Journal*, Vol. 28, No. 4, April 1990, pp. 717–724, doi: 10.2514/3.10451

[31]Li, W. P. and Huang, H., "Integrated Optimization of Actuator Placement and Vibration Control for Piezoelectric Adaptive Trusses," *Journal of Sound and Vibration*, Vol. 332, No. 1, Jan. 2013, pp. 17–32, doi: 10.1016/j.jsv.2012.08.005

[32]Grandhi, R. V., "Structural and Control Optimization of Space Structures," *Computers & Structures*, Vol. 31, No. 2, 1989, pp. 139–150, doi: 10.1016/0045-7949(89)90222-8

[33]Belvin, W. K. and Park, K. C., "Structural Tailoring and Feedback Control Synthesis: An Interdisciplinary Approach," *Journal of Guidance, Control, and Dynamics*, Vol. 13, No. 3, May 1990, pp. 424–429, doi: 10.2514/3.25354

[34]Haftka, R. T. and Gürdal, Z., *Elements of Structural Optimization*, Vol. 11, Springer, 3rd ed., 1992, doi: 10.1007/978-94-011-2550-5

[35]Lai, E. and Ananthasuresh, G. K., "On the Design of Bars and Beams for Desired Mode Shapes," *Journal of Sound and Vibration*, Vol. 245, No. 2, July 2002, pp. 393–406, doi: 10.1006/jsvi.2001.4101

[36]Herber, D. R., McDonald, J. W., Alvarez-Salazar, O. S., Krishnan, G., and Allison, J. T., "Reducing Spacecraft Jitter During Satellite Reorientation Maneuvers via Solar Array Dynamics," *AIAA/ISSMO Multidisciplinary Analysis and Optimization Conference*, No. AIAA 2014-3278, Atlanta, GA, USA, June 2014, doi: 10.2514/6.2014-3278

[37]Yu, Y.-Q., Howell, L. L., Lusk, C., Yue, Y., and He, M.-G., "Dynamic Modeling of Compliant Mechanisms Based on the Pseudo-Rigid-Body Model," *Journal of Mechanical Design*, Vol. 127, No. 4, Aug. 2005, pp. 760–765, doi: 10.1115/1.1900750

[38]Ben-Tal, A. and Bar-Yoseph, P. Z., "Space-Time Spectral Element Method for Optimal Slewing of a Flexible Beam," *International Journal for Numerical Methods in Engineering*, Vol. 39, No. 18, Sept. 1996, pp. 3101–3121, doi: 10.1002/(SICI)1097-0207(19960930)39:18<3101::AID-NME987>3.0.CO;2-O

[39]Bisplinghoff, R. L., Ashley, H., and Halfman, R. L., *Aeroelasticity*, Addison-Wesley, 1995.

[40]Junkins, J. L. and Kim, Y., *Introduction to Dynamics and Control of Flexible Structures*, AIAA, 1st ed., 1993, doi: 10.2514/4.862076

[41]Paranjape, A. A., Guan, J., Chung, S.-J., and Krstic, M., "PDE Boundary Control for Flexible Articulated Wings on a Robotic Aircraft," *IEEE Transactions on Robotics*, Vol. 29, No. 3, June 2013, pp. 625–640, doi: 10.1109/TRO.2013.2240711

[42]Deshmukh, A. P., Herber, D. R., and Allison, J. T., "Bridging the Gap between Open-Loop and Closed-Loop Control in Co-Design: A Framework for Complete Optimal Plant and Control Architecture Design," *American Control Conference*, Chicago, IL, USA, July 2015, pp. 4916–4922, doi: 10.1109/ACC.2015.7172104

[43]Enright, P. J. and Conway, B. A., "Discrete Approximations to Optimal Trajectories Using Direct Transcription and Nonlinear Programming," *Journal of Guidance, Control, and Dynamics*, Vol. 15, No. 4, July–Aug. 1992, pp. 994–1002, doi: 10.2514/3.20934

[44]Betts, J. T., *Practical Methods for Optimal Control and Estimation Using Nonlinear Programming*, SIAM, 2nd ed., 2010, doi: 10.1137/1.9780898718577

[45]Biegler, L. T., *Nonlinear Programming: Concepts, Algorithms, and Applications to Chemical Processes*, SIAM, 2010, doi: 10.1137/1.9780898719383

[46]Chilan, C. M. and Conway, B. A., "Automated Design of Multiphase Space Missions Using Hybrid Optimal Control," *Journal of Guidance, Control, and Dynamics*, Vol. 36, No. 5, Sept. 2013, pp. 1410–1424, doi: 10.2514/1.58766

[47]Morgan, D., Chung, S.-J., and Hadaegh, F. Y., "Model Predictive Control of Swarms of Spacecraft Using Sequential Convex Programming," *Journal of Guidance, Control, and Dynamics*, Vol. 37, No. 6, 2014, pp. 1725–1740, doi: 10.2514/1.G000218

[48]Herber, D. R., *Dynamic System Design Optimization of Wave Energy Converters Utilizing Direct Transcription*, M.S. Thesis, University of Illinois at Urbana-Champaign, Urbana, IL, USA, May 2014.

[49]Deshmukh, A. P. and Allison, J. T., "Multidisciplinary Dynamic Optimization of Horizontal Axis Wind Turbine Design," *Structural and Multidisciplinary Optimization*, 2015, doi: 10.1007/s00158-015-1308-y

[50]Paranjape, A. A., Chung, S.-J., Hilton, H. H., and Chakravarthy, A., "Dynamics and Performance of Tailless Micro Aerial Vehicle with Flexible Articulated Wings," *AIAA Journal*, Vol. 50, No. 5, May 2012, pp. 1177–1188, doi: 10.2514/1.J051447

[51]Moheimani, S. O. M. and Fleming, A. J., *Piezoelectric Transducers for Vibration Control and Damping*, Springer, 1st ed., 2006, doi: 10.1007/1-84628-332-9

[52]Erdman, A. and Sandor, G., *Mechanism Design: Analysis and Synthesis*, Prentice Hall, 4th ed., 2001.

[53]Patterson, M. A. and Rao, A. V., "GPOPS–II: A MATLAB Software for Solving Multiple-Phase Optimal Control Problems Using hp-Adaptive Gaussian Quadrature Collocation Methods and Sparse Nonlinear Programming," *ACM Transactions on Mathematical Software*, Vol. 41, No. 1, Oct. 2014, doi: 10.1145/2558904

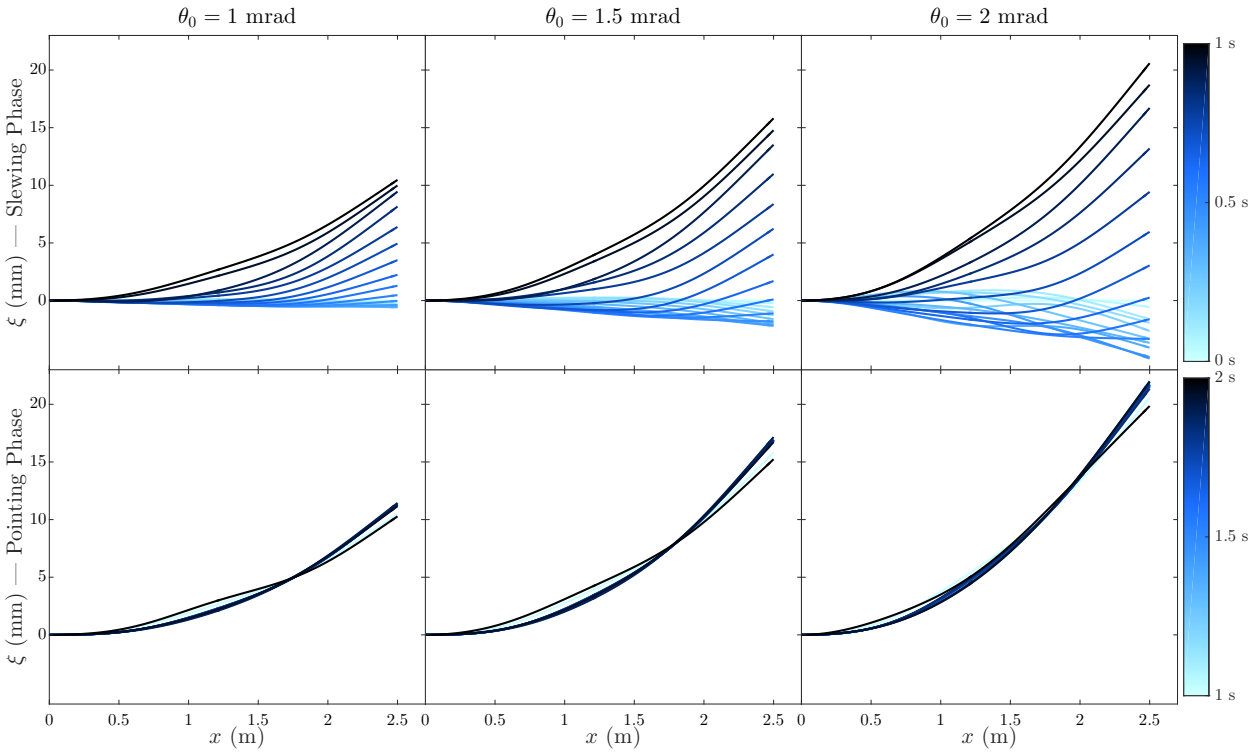

Figure 10: Beam deflection profiles for select values of θ_0 with variable length (VL) and nominal mass.

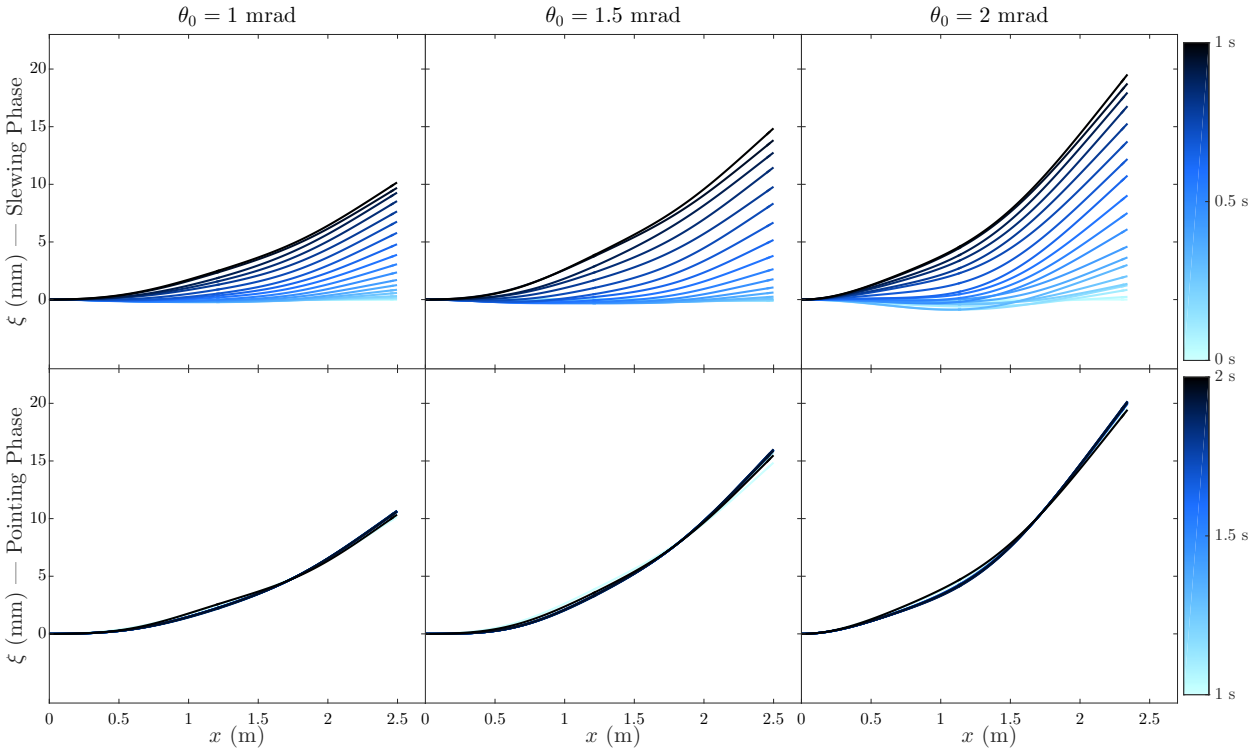

Figure 11: Beam deflection profiles for select values of θ_0 with piecewise linear segments (PLS) and nominal mass.

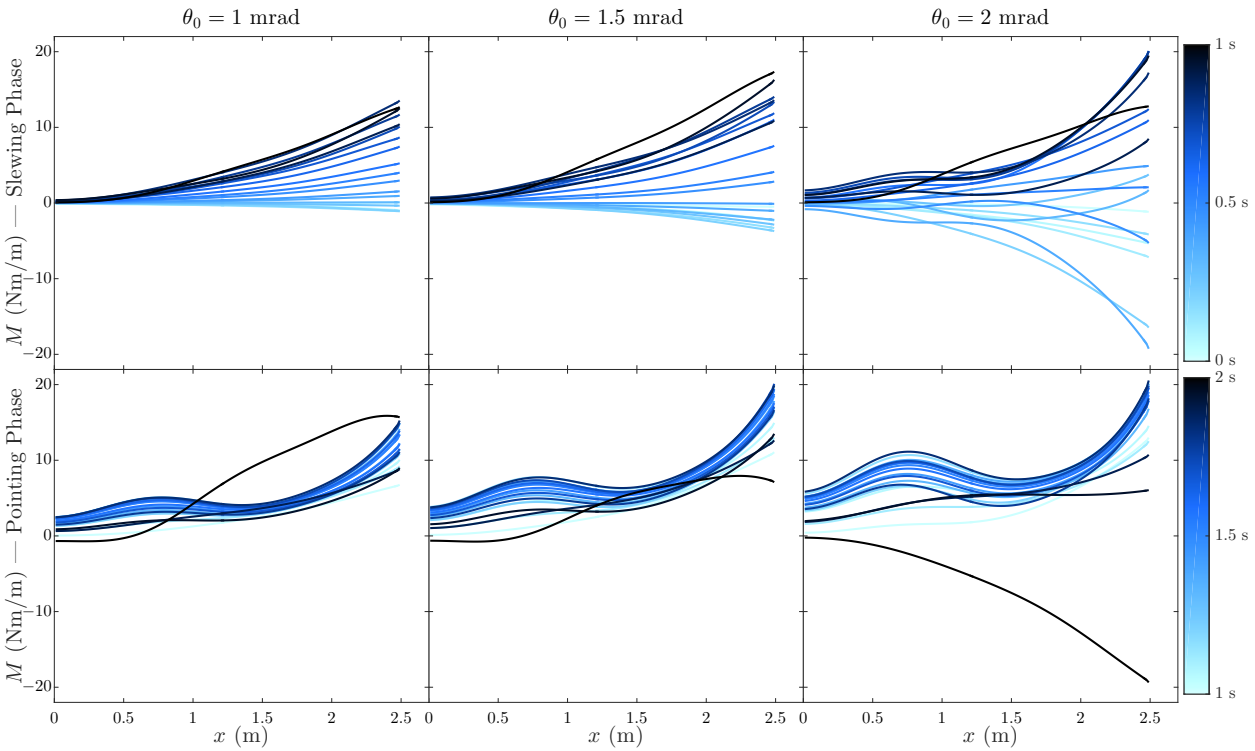

Figure 12: Spatially varying moment profiles for select values of θ_0 with variable length (VL) and nominal mass.

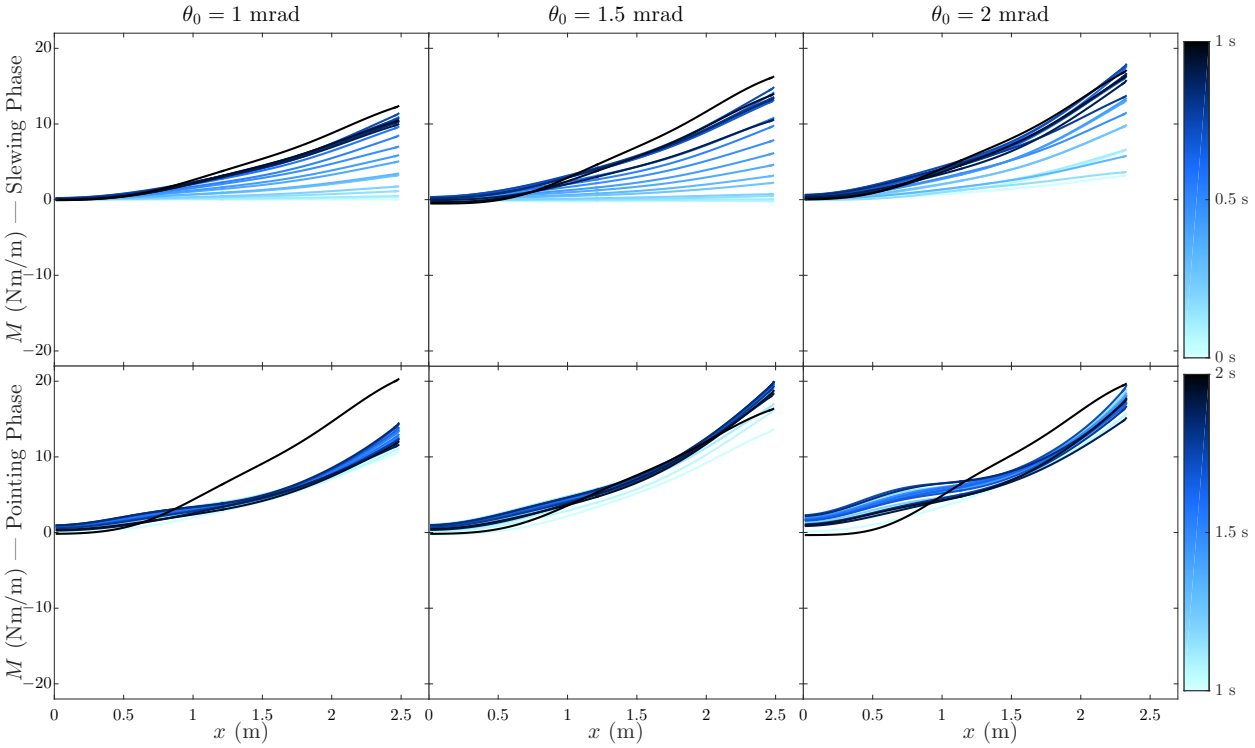

Figure 13: Spatially varying moment profiles for select values of θ_0 with piecewise linear segments (PLS) and nominal mass.